JGR Atmospheres

RESEARCH ARTICLE
10.1029/2020JD033963

Key Points:

- The main factors influencing local CH_4 values at Hegyhátsál (HUN) are local meteorology, and seasonal anthropogenic emissions related to heating
- The HUN station is valuable for monitoring local and regional methane emissions and tracking source inputs
- CH_4 increments and isotopic seasonality in air at the Hungarian continental background site are comparable to other European regional sites

Supporting Information:

Supporting Information may be found in the online version of this article.

Correspondence to:

E. László and T. Varga,
laszlo.elemer@atomki.hu;
varga.tamas@atomki.hu

Citation:

Varga, T., Fisher, R. E., France, J. L., Haszpra, L., Jull, A. J. T., Lowry, D., et al. (2021). Identification of potential methane source regions in Europe using $\delta^{13}C_{CH4}$ measurements and trajectory modeling. *Journal of Geophysical Research: Atmospheres*, *126*, e2020JD033963. https://doi.org/10.1029/2020JD033963

Received 16 OCT 2020
Accepted 23 AUG 2021

Author Contributions:

Conceptualization: T. Varga, L. Haszpra, D. Lowry, E. G. Nisbet, E. László
Data curation: L. Haszpra, D. Lowry, M. Molnár
Formal analysis: R. E. Fisher, D. Lowry, I. Major, M. Molnár, E. G. Nisbet
Funding acquisition: E. G. Nisbet
Investigation: T. Varga, L. Haszpra, D. Lowry, E. G. Nisbet, E. László
Methodology: T. Varga, J. L. France, L. Haszpra, D. Lowry, E. G. Nisbet, E. László
Resources: L. Haszpra
Software: E. László

Identification of Potential Methane Source Regions in Europe Using $\delta^{13}C_{CH4}$ Measurements and Trajectory Modeling

T. Varga[1,2], R. E. Fisher[3], J. L. France[3,4], L. Haszpra[5], A. J. T. Jull[1,6,7], D. Lowry[3], I. Major[1], M. Molnár[1], E. G. Nisbet[3], and E. László[1]

[1]Isotope Climatology and Environmental Research Centre (ICER), Institute for Nuclear Research (ATOMKI), Debrecen, Hungary, [2]Doctoral School of Physics, University of Debrecen, Debrecen, Hungary, [3]Department of Earth Sciences, Royal Holloway, University of London, Egham, UK, [4]British Antarctic Survey, Natural Environment Research Council, Cambridge, UK, [5]Research Centre for Astronomy and Earth Sciences, Geodetic and Geophysical Institute, Sopron, Hungary, [6]Department of Geosciences, University of Arizona, Tucson, AZ, USA, [7]University of Arizona AMS Laboratory, Tucson, AZ, USA

Abstract The methane emissions from the Hungarian Pannonian Basin are not well qualified, due to a lack of measurements of CH_4 mole fraction and $\delta^{13}C_{CH4}$ in the air. This study reports methane measurements in air samples from Hungary, placing them in the context of regional and global background data, to investigate the inputs to the methane burden in Central Europe. CH_4 mole fraction and $\delta^{13}C_{CH4}$ from the Hungarian tall tower station, Hegyhátsál, and additional data from Mace Head (Ireland) and Zeppelin (Svalbard) are used with back trajectory modeling to identify central European source areas and their seasonal variation between the summer vegetation and winter heating periods. Methane measurements in air masses sampled in the European interior, have significantly higher maxima and seasonal amplitudes than at the Mace Head and Zeppelin European background sites. The mean CH_4 mole fraction value is about 80 ppb higher than the comparable marine background, and values above 2,000 ppb were frequently observed between February 2013 and December 2015. The mean $\delta^{13}C_{CH4}$ value -47.5 ± 0.3‰ (2σ) was comparable to values at all three monitoring sites, but specific pollution events were detected at Hegyhátsál. Concentration weighted trajectory modeling, meteorological parameters, stable carbon isotopic composition ($\delta^{13}C_{CH4}$), and Miller-Tans analysis show that the main factors influencing CH_4 at the Hegyhátsál, apart from diurnal and seasonal changes in the planetary boundary layer, are emissions from residential heating and industrial CH_4 emissions during the winter.

1. Introduction

Since 2007, the methane burden in the global atmosphere has increased significantly (Dlugokencky, 2021). Methane (CH_4) has the second-largest radiative forcing impact among the anthropogenic greenhouse gases (Etminan et al., 2016; IPCC, 2018) besides CO_2. The increase in the methane burden has been sustained since the industrial revolution, except for a short stable period between 1999 and 2006, more than doubling relative to the preindustrial level (Nisbet et al., 2019; Saunois et al., 2020). Methane's growth rate and seasonality depend on both the seasonal and inter-annual changes in emission fluxes from the various anthropogenic and natural sources and also potentially in methane sinks (Saunois et al., 2016). Globally, the largest emitters are wetlands, agricultural emissions, especially ruminant enteric fermentation and manure, fossil fuel, fire emissions, sewage and waste disposal (Dlugokencky et al., 2011; Saunois et al., 2016; Schaefer et al., 2016). The main sink of atmospheric methane is oxidation by tropospheric hydroxyl. Minor sinks are loss to the stratosphere, tropospheric chlorine radicals, and soil and karst methanotrophy (Dlugokencky et al., 2011; Mattey et al., 2013; Nisbet et al., 2019; Webster et al., 2018).

Methane's renewed growth since 2007, especially in the tropics, has been accompanied by a concurrent isotopic shift to lighter $\delta^{13}C_{CH4}$. This may be driven by changes in thermogenic and biogenic methane emission sources, but changes in sinks may also have occurred (Nisbet et al., 2019; Rigby et al., 2017; Turner et al., 2017; Worden et al., 2017). CH_4 mole fraction time-series, by themselves, provide limited information to solve regional budgets, thus other information is required to detect emission sources.

Supervision: E. László
Validation: E. László
Visualization: T. Varga, J. L. France, E. László
Writing – original draft: T. Varga, D. Lowry, E. G. Nisbet, E. László
Writing – review & editing: T. Varga, L. Haszpra, A. J. T. Jull, D. Lowry, I. Major, E. G. Nisbet, E. László

The $\delta^{13}C_{CH4}$ carbon isotopic composition of methane contains powerful information about source inputs since the different sources have specific $\delta^{13}C_{CH4}$ signatures (Brownlow et al., 2017; Fisher et al., 2017; France et al., 2016; Górka et al., 2014; Kirschke et al., 2013; Schwietzke et al., 2016; Tyler et al., 2007; Zazzeri et al., 2016, 2017). The three main types of CH_4 emissions have characteristically distinct $\delta^{13}C_{CH4}$ signatures, ranges: -61.7 ± 6.2‰ for modern microbial sources, -44.8 ± 10.7‰ for fossil fuel sources, -26.2 ± 4.8‰ for biomass burning, depending on whether the fuel is C4 plant matter (e.g., maize crop waste) or isotopically more negative C3 material (e.g., trees and bushes) (Sherwood et al., 2017). This data set shows that the ranges of $\delta^{13}C_{CH4}$ ratios of thermogenic (fossil fuel) sources and biogenic (modern microbial) source overlap, which needs to be considered during the interpretation. The mean global bulk source $\delta^{13}C_{CH4}$ is between -54 and -52‰, while, with fractionation by sink processes, the $\delta^{13}C_{CH4}$ signature of background ambient air varies between about -47.8 and -47.2‰ (Nisbet et al., 2016, 2019), depending on latitude and season. Mole fraction and isotopic ratio analyses coupled with atmospheric modeling (using backward air mass trajectories) provide tools for identification of sources and understanding of atmospheric processes responsible for concentration changes and isotopic shifts (Menoud et al., 2020; Röckmann et al., 2016). Menoud et al. (2020) and Röckmann et al. (2016) used high-resolution data for CH_4 mole fraction, $\delta^{13}C_{CH4}$ and δD_{CH4}, associated with model calculations in Europe (Lutjewad and Cabauw, Netherland), to reveal local and regional CH_4 emission sources. Back trajectories help identify the potential source regions of specific air masses and can help to reveal the production processes of regional and local increments to atmospheric CH_4 (France et al., 2016; García et al., 2016; Menoud et al., 2020; Röckmann et al., 2016).

Our aim is to identify significant CH_4 source areas in central Europe, by applying sector analysis to discrete methane mole fraction and $\delta^{13}C_{CH4}$ time-series data from the Hegyhátsál (Pannonian Basin, Hungary) tall tower greenhouse gas monitoring station (NOAA code: HUN) (Bergamaschi et al., 2018; Haszpra et al., 2005, 2008; Major et al., 2018). This HUN site samples air inputs from the agricultural plains at the Pannonian Basin, while large-scale transport brings air from the wider region of the north and western European regions. Data for the period 2013–2015 from Hegyhátsál are compared with contemporaneous data from six European and one Northern American stations (Figure 1, Table 1). Back trajectories were calculated using NOAA's Hybrid Single Particle Lagrangian Integrated Trajectory Model (HYSPLIT, https://www.ready.noaa.gov/HYSPLIT.php) to identify the source regions methane inputs into specific air masses and to locate emission source areas.

2. Materials and Methods

2.1. Study Area

Hegyhátsál rural, tall tower sampling station (HUN) is in western Hungary (46.95°N, 16.65°E, 248 m asl). The air inlet is 96 meters above ground level. Samples were typically collected in mid-afternoon (Table S1), when the well-mixed planetary boundary layer was deepest. The sampling time was around 1 min to fill the 3 L Tedlar bags. Between one and four samples were collected every month from February 2013 to December 2015.

The climate of the region is temperate continental and the surrounding area is dominated by arable agricultural fields, as well as some pastures and forests. Industrial activity is negligible in the region and the closest roads are also free of heavy traffic. Local emissions in the Pannonian Basin area are primarily from agriculture, waste disposal, traffic, and use of natural gas (Haszpra et al., 2005, 2008; Major et al., 2018). The prevailing wind blows from the northwest (Radics & Bartholy, 2008). The average wind speed is within the 2–3 m/s interval at HUN site and slightly increases with height (Bartholy & Radics, 2005). The frequency of occurrence (number of events) of anticyclonic conditions on an annual basis is 49.6% of the time, with 50.4% cyclonic, according to the objective Maheras classification. Season-wise, the frequency of the anticyclones (cyclones) types is in winter 39.1% (60.9%), in spring 42.0% (58.0%), in summer 64.7% (35.3%) and in autumn 52.1% (47.9%) (Maheras et al., 2018).

2.2. Mole Fraction and Stable Isotope Measurements

CH_4 mole fraction measurements at the department of Earth Sciences, Royal Holloway, University of London (RHUL) were by a Picarro G1301 cavity ring-down analyzer, to the WMO X2004A scale. Stable carbon

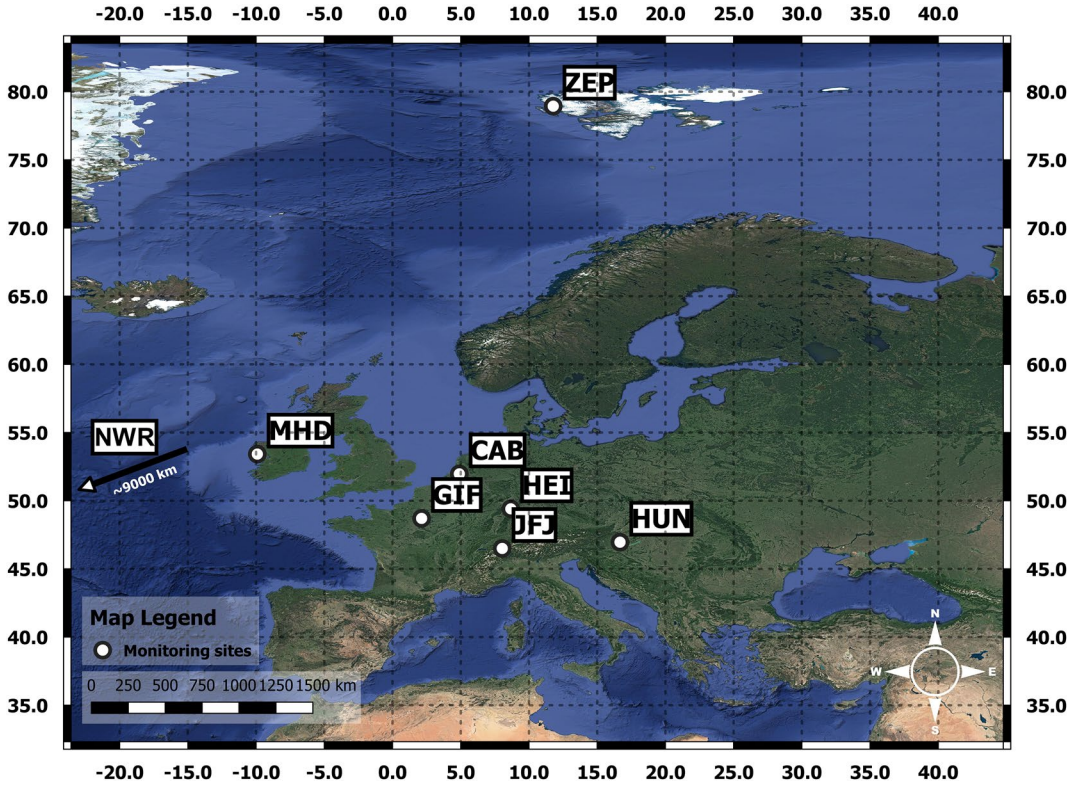

Figure 1. Location of the monitoring sites involved in this study for the comparison with HUN site. Mace Head, Ireland; Hegyhátsál, Hungary; Zeppelin, Svalbard, Heidelberg, Gif-sur-Yvette, Niwot Ridge, Jungfraujoch and Cabauw.

isotope ratio ($\delta^{13}C_{CH4}$) measurements of the Hegyhátsál samples were carried out using a GC-IRMS technique (Fisher et al., 2006; Nisbet et al., 2016, 2019). Reproducibility is 0.05‰ or better for most $\delta^{13}C_{CH4}$ measurements. The $\delta^{13}C$ values are calculated using the following equation (Quay et al., 1991):

$$\delta^{13}C(‰) = \left(\frac{\left(^{13}C/^{12}C\right)_{sample}}{\left(^{13}C/^{12}C\right)_{standard}} - 1 \right) \times 1000 \quad (1)$$

In order to determine the "local" additional methane source whilst also taking into account the background variation in the atmospheric $\delta^{13}C_{CH4}$ and mixing ratio a Miller-Tans style approach was undertaken (Miller & Tans, 2003). Each measurement is manually assigned an earlier point to act as a background, with the background chosen as close in time as possible to the measurement whilst also following the baseline trend for $\delta^{13}C_{CH4}$ and mixing ratio for that site. The resulting datasets for each site were plotted as Miller-Tans

Table 1
The Stations Used for the Comparison With the HUN Site are Listed in the Table

Station	Code	Lat	Lon	m asl	Reference
Mace Head	MHD	53.33°N	9.90°W	26	NOAA/Dlugokencky et al. (2019); White et al. (2018)
Zeppelin	ZEP	78.91°N	11.88°E	475	NOAA/Dlugokencky et al. (2019); White et al. (2018)
Niwot Ridge	NWR	40.05°N	105.59°W	3,523	NOAA/Dlugokencky et al. (2019); White et al. (2018)
Heidelberg	HEI	49.42°N	8.68°E	116	ICOS/InGOS (2015a)
Gif-sur-Yvette	GIF	48.71°N	2.15°E	167	ICOS/InGOS (2015b)
Jungfraujoch	JFJ	46.55°N	7.99°E	3,580	ICOS/InGOS (2015c)
Cabauw	CAB	51.97°N	4.93°E	213	Röckmann et al. (2016)

plots, where the slope of the linear regression represents the source $\delta^{13}C_{CH4}$ signature (Lowry et al., 2020; Miller & Tans, 2003).

2.3. HYSPLIT Modeling and Concentration Weighted Trajectory Calculations

HYSPLIT backward trajectories were calculated from the starting time, location, and height of each sampling campaign (Draxler, 1998; Su et al., 2015), using the Archive Global Data Assimilation System meteorological data set (GDAS 0.5°) to model −72-hr-long trajectories to investigate air mass provenance and the source regions of input emissions. One trajectory was calculated for every sampling time, although the resolution of the GDAS data set is 3 h and the sampling time was around 1 min. Concentration weighted trajectory (CWT) maps with 2° resolution grid cells were produced by the Trajstat plugin of METEOINFO software (Hsu et al., 2003; Wang et al., 2009), based on the trajectories coupled with measured methane mole fraction and $\delta^{13}C_{CH4}$ data. Grid cells containing less than four trajectories were excluded. The most remote 15% (by distance) of each trajectory was also excluded, to concentrate on the closer emission source regions and reduce the uncertainty of the results. The CWT calculations were produced by the following formula:

$$C_{ij} = \frac{1}{\sum_{l-1}^{M} \tau_{ijl}} \sum_{l-1}^{M} C_l \tau_{ijl} \tag{2}$$

where C_{ij} is the average weighted concentration in the ijth cell, l is the index of the trajectory, M is the total number of trajectories, C_l is the concentration observed on the arrival of trajectory l, and τ_{ijl} is the time trajectory l spent in the ijth cell. (Wang et al., 2009). In the case of calculation of the $\delta^{13}C_{CH4}$ -weighted map, the C_l is the $\delta^{13}C_{CH4}$ value observed on the arrival of trajectory l, C_{ij} is the average weighted $\delta^{13}C_{CH4}$.

2.4. Cross-Correlation Analysis of CH_4 Mole Fraction and Planetary Boundary Layer Height

Cross-correlation is used to analyze isotopic and meteorological time series (László et al., 2020; Palcsu et al., 2018). To analyze the relationship between planetary boundary layer height and CH_4 mole fraction, a Pearson linear correlation coefficient was calculated according to Equation 3.

$$r_m = \frac{\Sigma\left(x_i - \overline{x}\right)\left(y_{i-m} - \overline{y}\right)}{\sqrt{\Sigma\left(x_i - \overline{x}\right)^2 \Sigma\left(y_{i-m} - \overline{y}\right)^2}} \tag{3}$$

where two time-series x and y and the cross-correlation value at each lag time m is calculated. The summations and mean values in the equation are extended only over the overlapped segment, where the value of cross-correlation changes with a given lag time. In the case of positive lags, x is compared with a y that has been delayed by m samples. Strong correlation value at positive lags thus means that features in y are leading, while x lags behind (Davis, 1986). Cross-correlation significance has been performed with a random-phase test (Ebisuzaki, 1997).

3. Results and Discussion

3.1. Temporal and Spatial Variation of CH_4 Mole Fraction and $^{13}C_{CH4}$ Values

The measured methane mole fraction in ambient air at the HUN station is generally greater than at Mace Head, Ireland (MHD) and Zeppelin, Svalbard (ZEP) (Figures 2a, 2b, 4a, and 4b). Between 2013 and 2015, the mean CH_4 mole fraction was 1,984 ± 48 ppb at the HUN station, compared to 1,908 ± 22 ppb at MHD and 1,901 ± 22 ppb at ZEP (all errors to 1σ). The range of measured CH_4 mole fraction values is wider at HUN site than at MHD or ZEP. In particular, values higher than 2,000 ppb at HUN station were often observed during the monitoring campaign, and the frequency distribution is flatter (Figure 4a).

The seasonal variation in methane has much greater amplitude at HUN than at MHD and ZEP, which is both consistent with the proximity to HUN of several seasonally intensive methane emission sources, and also because the thickness of the planetary boundary layer and the height of the inversion vary more intensely at the HUN continental interior site (Figure S1a), compared to the marine settings of the background stations (Engeln & Teixeira, 2013; Stull, 1988). At HUN, the highest CH_4 values were measured in

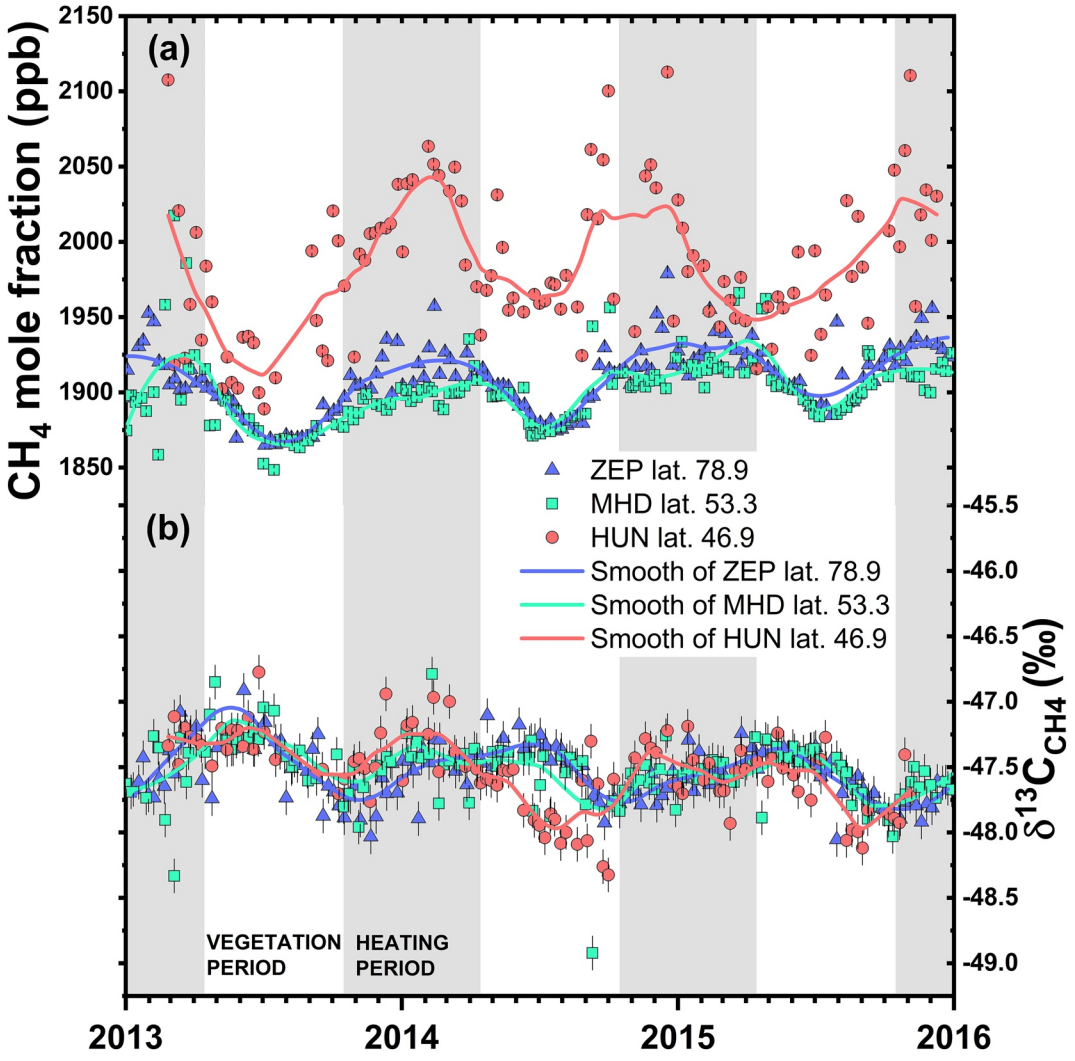

Figure 2. (a) Methane, and $\delta^{13}C_{CH4}$ stable isotope ratio (b) time series of HUN, MHD, and ZEP monitoring stations. Colored dots show sample CH_4 mole fraction and $\delta^{13}C$ isotope ratio. The colored lines show the smoothed data of individual measurement values (data set were smoothed by the Lowess filter method in the Origin 2020b software) to guide the eye and visualization of the seasonal changes. The gray shaded areas show the heating period in Hungary.

winter and occurred simultaneously with high carbon monoxide (Petron et al., 2019), which is consistent with emissions from incomplete combustion processes during the heating period. The source signatures of the vegetation and heating periods are further discussed below by Miller-Tans plots and trajectory analysis. The lowest CH_4 values were observed in summer, following the zonal (Northern Hemisphere) seasonality of methane destruction by OH and also the absence of heating emissions in summer (Figure 2a), however, wetland related CH_4 emissions also strongly influence the amplitude and phase (Fung et al., 1991).

The maximum CH_4 mole fraction observed was 2,113 ppb (December 12th, 2014) at the HUN station, significantly higher than maxima in the marine background at ZEP (1,978 ppb on December 18th, 2014) and MHD (2,017 ppb on March 6th, 2013). During the time period of the observations, CH_4 mole fraction values above 1,950 ppb were rare at other NOAA marine and polar stations, unlike at the HUN site. The yearly minima at the HUN site are 32–53 ppb higher than at MHD, while the yearly maxima are 90–156 ppb higher at HUN. Annual values of CH_4 and $\delta^{13}C_{CH4}$ are shown in the Table S2. For 2013 there are no data before March or for late summer, so it is likely that the annual average is biased toward ^{13}C enrichment. Annual average CH_4 mole fraction of the monthly mean of discrete samples at the HUN station increased by 22 ppb

between 2013 and 2015. In the case of the MHD site, this increase was 22 ppb (2013–2015), while 21 ppb of growth was observed at ZEP station during the same time period.

As is widely observed in inland sites, there is typically a strong diurnal cycle of the CH_4 mole fraction at HUN, which depends on the height of the planetary boundary layer (PBL). When the PBL height is low, the CH_4 mole fraction is high and vice versa (Figure S1b), reflecting the accumulation of methane emitted locally at the surface in the shallow boundary layer (Haszpra et al., 2019), mostly overnight. At marine sites, in free-flowing air from the ocean with a lack of local emission sources, this diurnal cycle is typically less pronounced, an observation shown by the cross-correlation coefficient at the MHD and ZEP sites (Figure S1b). At HUN site, strong negative correlation was observed between PBL and CH_4 mole fraction with a 0-month delay, while at the other sites, strong positive correlation was observed. HUN is out of phase with the MHD and ZEP sites.

Comparison with methane mole fraction at the Niwot Ridge, NOAA (NWR) and Jungfraujoch (JFJ) continental background sites shows that the HUN station is not appropriate for a continental background station, as the NWR and JFJ sites have better clean air sectors and are not as burdened with local emissions as the HUN site (Dlugokencky et al., 2021; InGOS, 2015c). During 2013–2015, while the mean CH_4 mole fractions at the NWR and JFJ station are 1,876 ± 26 and 1,895 ± 25 ppb, the mean CH_4 mole fraction is 1,984 ± 48 ppb at the HUN site (Figure S2a). The mentioned continental background sites are located at higher altitudes, the NWR site is located at 3,523 m asl, the JFJ site is located at 3,580 m asl, while the HUN station is located much closer to the emission sources, at 248 m asl. The JFJ and NWR sites are in the well-mixed troposphere and not in the frequently poorly mixed boundary layer. Although the mean CH_4 mole fraction value at HUN between 2013 and 2015 is higher, the amplitude and maxima are lower than at the Heidelberg and Gif-sur-Yvette stations, where the mean CH_4 mole fraction was 1,959 ± 55 and 1,956 ± 58 ppb (InGOS, 2015a, 2015b), and the maximal value was 2,564 and 2,293 ppb respectively, compared to 2,113 ppb at the HUN site. Based on these, the HUN site is less affected by local emissions than the Heidelberg and Gif-sur-Yvette sites. In Cabauw (Netherlands) Röckmann et al. (2016) measured even higher CH_4 mole fractions (greater than 2,250 ppb was often observed in this study carried out in 2013–2014), showing strong local or near region methane inputs (Figure S2a). Note that our data are based on discrete spot sampling (between one and four samples per month) and will miss most events. In contrast, the Heidelberg and Gif-sur-Yvette data have 1 h time resolution, and the time resolution of the data presented in Röckmann et al. (2016) is 1.5 h or higher.

Unlike the CH_4 mole fraction data, $\delta^{13}C_{CH4}$ values for the HUN site and the MHD and ZEP global background monitoring network stations show a comparable range and temporal variation, although high values can be observed at all sites (Figures 2, 3 and 4b). Mean $\delta^{13}C_{CH4}$ values and their 2σ standard deviation are similar at the three stations: −47.5 ± 0.4‰ (ZEP), −47.5 ± 0.5‰ (MHD), and −47.5 ± 0.6‰ (HUN) (the error is the 2σ stdev of the measurements over the investigated period), and are within the ranges recorded for background ambient air (between −47.8 and −47.2‰) (Nisbet et al., 2016, 2019). Our measured data at HUN compared to the NWR background site shows that $\delta^{13}C_{CH4}$ values are in a similar interval, but $\delta^{13}C_{CH4}$ values at NWR are generally higher than the mean value at HUN (Dlugokencky et al., 2019). This can be due to the differences between the continental source regions and source mixes at North America and Europe (Chang et al., 2019; Ganesan et al., 2018; Sherwood et al., 2017). Worthy of note that there is regional variability in the isotopic signature of wetland, fossil fuel and ruminant emissions. Therefore, the mole fraction value can be similar at HUN and NWR, but the $\delta^{13}C_{CH4}$ can be different, and the $\delta^{13}C_{CH4}$ very similar at the European sites (HUN, MHD, ZEP), due to the different source mixes. The $\delta^{13}C_{CH4}$ signal at the Cabauw site is generally strongly depleted, associated with higher CH_4 mole fractions compared to the HUN site (Figure S2), which shows that Cabauw, which is in an agricultural setting, is more affected by local and regional methane sources than HUN (Röckmann et al., 2016). At HUNPositive $\delta^{13}C_{CH4}$ shifts greater than 0.2‰ were observed in March and November of 2013, and September and October of 2014. Negative $\delta^{13}C_{CH4}$ shifts greater than −0.2‰ were recorded during the vegetation-growth periods, presumably due to the higher biogenic emission in this period.

During winter, the CH_4 mole fraction is elevated. The PBL was deeper during the end of the winter of 2014–2015 compared to the previous year (winter of 2013–2014), and as the deeper PBL favors the lower CH_4 mole fraction, the yearly CH_4 mole fraction maximum shifted to earlier (Figures 2b, S2 and S3). During the

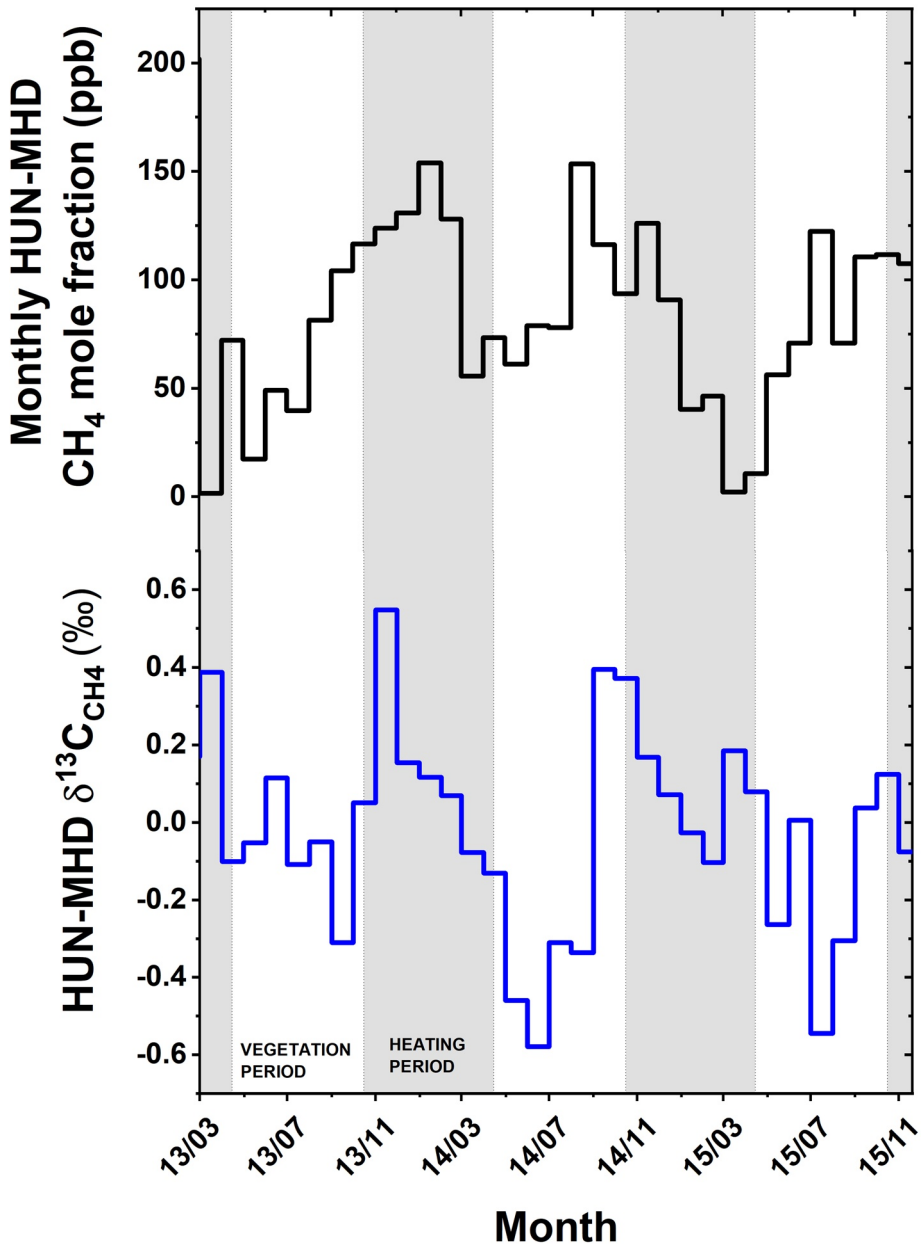

Figure 3. Difference in the CH_4 mole fraction and $\delta^{13}C_{CH4}$ ratio between the monthly average values at Hegyhátsál, Hungary (HUN) and Mace Head, Ireland (MHD) sites. The colored lines show differences between HUN and MHD sites of the monthly average values of CH_4 mole fraction (black) and $\delta^{13}C_{CH4}$ ratio (blue). Gray shaded areas show the heating period in Hungary.

winter heating period of 2014 and 2015, positive $\delta^{13}C_{CH4}$ shifts were observed at the HUN site, likely due to local fossil fuel and biomass related pyrogenic emissions, both of which are isotopically enriched in $^{13}C_{CH4}$ compared to the bulk atmospheric methane burden (Sherwood et al., 2017). The energy source for residential heating during the winter in European Union (EU) is mainly fossil natural gas (~40%) and oil (~15%). The use of coal has decreased since the 1990s, and now only supplies about 5% of the residential heating in EU. However, use of biomass burning for heating is increasing and provided about ~20% of building heat in 2015. The other ~20% is electricity and district heating (Bertelsen & Mathiesen, 2020). The source of the electricity and district heating can be nuclear or also coal, oil, and gas. The wetland related emission is dominant only at the North European, Scandinavian region, where the $\delta^{13}C_{CH4}$ signal is around −70‰, which is similar to the observed signal in the Canadian region (Ganesan et al., 2018). The ruminant CH_4 emission is

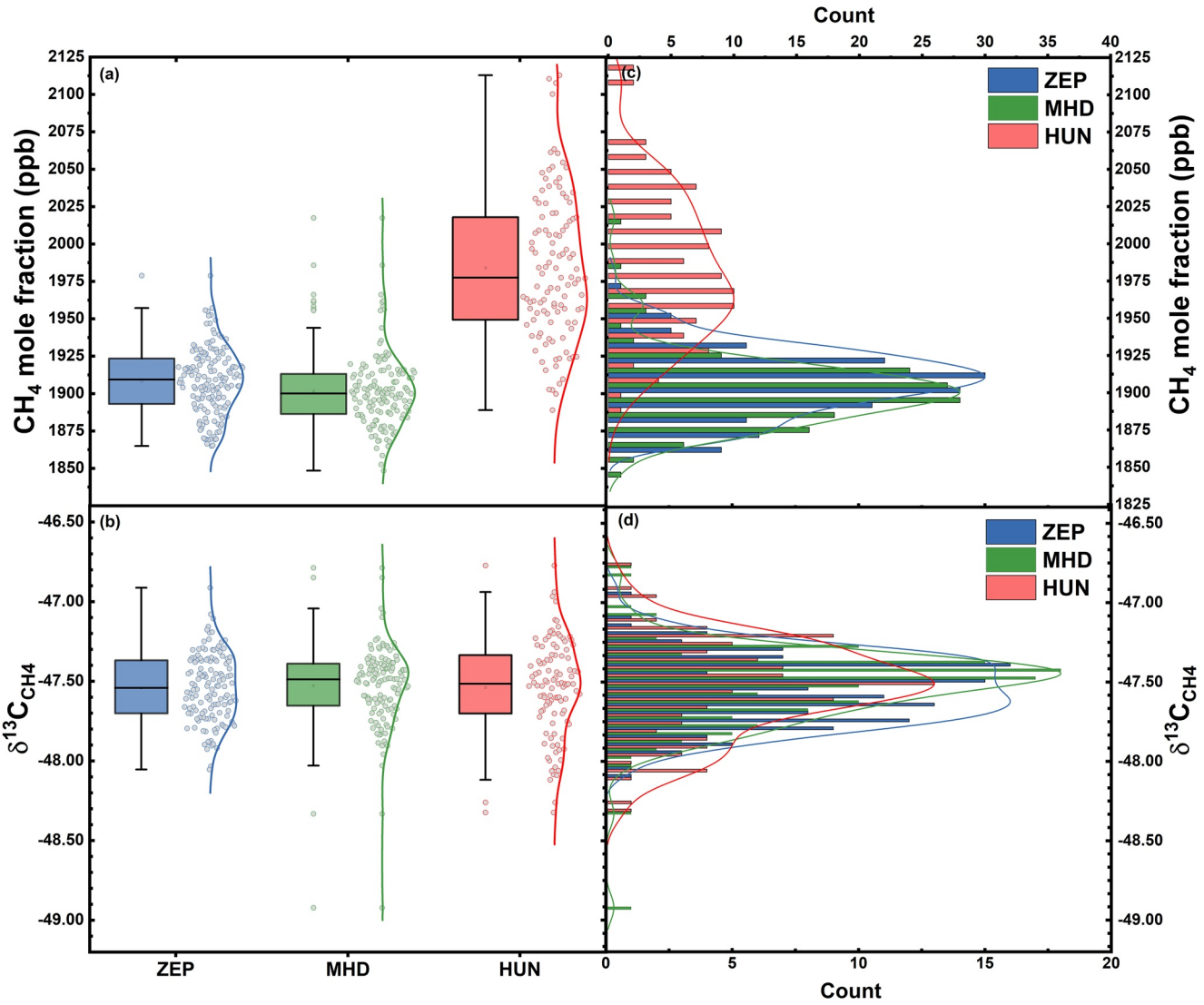

Figure 4. Box-plot of the CH_4 mole fraction (a) and $\delta^{13}C_{CH4}$ (b) values at the Zeppelin, Svalbard, Mace Head, Ireland, and Hegyhátsál, Hungary site. Histogram of CH_4 mole fraction (c) and $\delta^{13}C_{CH4}$ (d) at the different monitoring sites. The colored dots show the individual measurement values, the colored curves show the Kernel smoothed distribution curve of the values.

about 10 Tg/year in Europe, a few Tg higher than in the North Amerian region. The $\delta^{13}C$ signal of ruminant CH_4 emission in much of Europe is below −68‰, but when ruminants have a predominantly C4 diet it can be less depleted, as in the United States and China (Chang et al., 2019). The typical $\delta^{13}C_{CH4}$ signal of oil and natural gas CH_4 emission is under −40‰ in Europe (in Italy around −57‰) but in Hungary and the Netherlands, it is less depleted, around −38 and −33‰ (Sherwood et al., 2017).

During the summer vegetation period of 2014 and 2015, CH_4 at HUN was constantly about 50 ppb higher than at ZEP and MHD (Figures 2a and 3a). Monthly mean CH_4 mole fraction increments at the HUN site compared to MHD (Figure 3.) show generally higher values, up to 150 ppb higher. The increments are the highest at the heating period in January 2014 and during the vegetation period in August 2014. During the heating period in 2015, after a high increment in the vegetation period, HUN shows several months of low methane increment over the remote background stations. In the summer of 2014 and 2015, $\delta^{13}C_{CH4}$ trended more negative compared to ZEP and MHD, presumably due to emission from biogenic sources in central Europe, such as ruminants and wetlands, with strongly negative $\delta^{13}C_{CH4}$ (Fisher et al., 2017; Ganesan et al., 2018). Considering samples with $\delta^{13}C_{CH4}$ lower than −47.75‰ for the period between July 11th, 2014

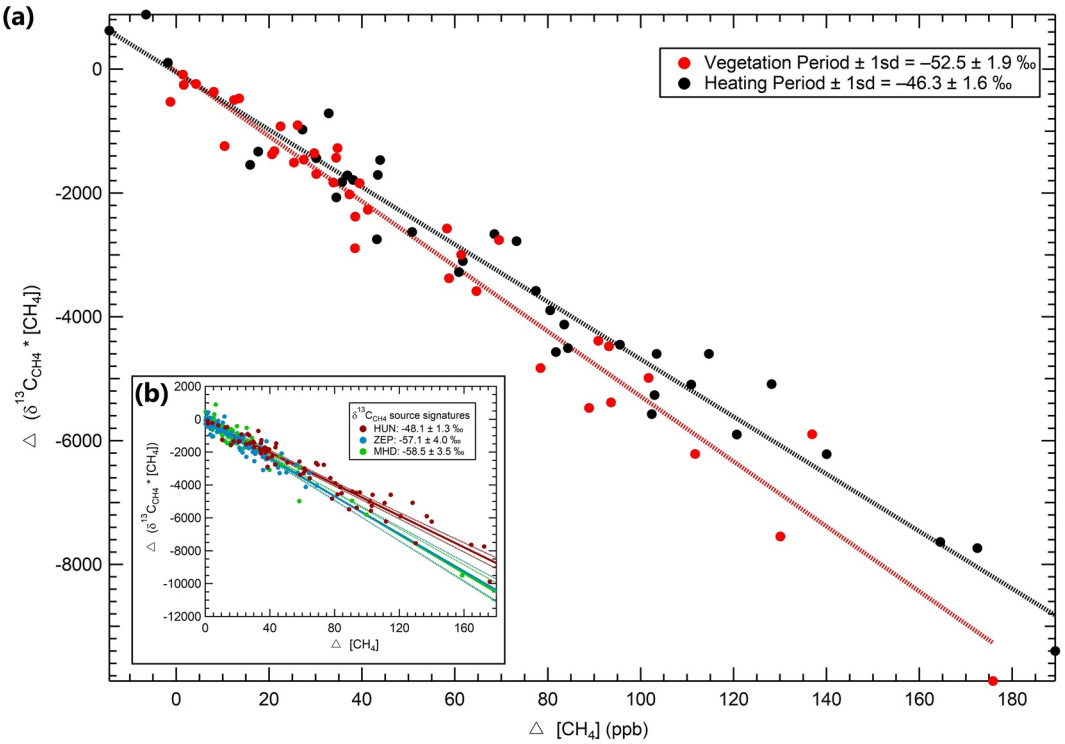

Figure 5. Miller-Tans plots showing the source signature of methane increments into background air. Collected from the Hegyhátsál, Hungary (HUN) site during the vegetation and heating periods separately (a) and for the whole investigated period at HUN, Mace Head, Ireland, and Zeppelin, Svalbard (b). The slopes show the dominant source signatures of incremental inputs at the different sites.

and October 8th, 2014, most sampled air masses moved slowly during the previous 72-hour and remained near ground level, within the PBL (Figures S4a–S4l). The implication is that the strongly negative $\delta^{13}C_{CH4}$ reflects inputs from local and proximal regional sources.

The Miller-Tans plot in Figure 5a shows enriched $\delta^{13}C_{CH4}$ in the heating period (−46.3 ± 1.6‰) compared to the observed −52.5 ± 1.9‰ signals in the vegetation period. This enriched signal associated with higher CH_4 mole fraction values during the heating period compared to the vegetation period, suggest a dominant fossil fuel origin for methane emission, as these are generally enriched in $^{13}C_{CH4}$ (Sherwood et al., 2017). Elevated carbon monoxide also suggests a dominant source of residential heating during the winter (Petron et al., 2019). The Miller-Tans plot in Figure 5b shows averaged input from sources that are ^{13}C-depleted relative to atmospheric background at all three monitoring sites. Values are quite similar for MHD and ZEP (−58.5 ± 3.5‰ and −57.1 ± 4.0‰) These are background stations with small source increments from distant sources, not proximal regional sources, but the source input for HUNis significantly more positive at −48.1 ± 1.3‰, and suggests contributions from European continental sources significantly richer in ^{13}C. This shows that the HUN station is not a clear, continental background station, but accesses air from regional methane sources. These results suggest that the dominant source mix adding incremental methane inputs into air arriving at HUN has a bulk isotopic signature more positive than the −53‰ value of the bulk global source (Nisbet et al., 2019). The local inputs sampled in the air masses reaching HUN are a mixture of both biogenic emissions (typically −55 to −70‰) and fossil fuel and pyrogenic emissions (typically −15 to −45‰). The mean $\delta^{13}C_{CH4}$ signal of coal and conventional gas CH_4 emission is around −45.7‰ in the European countries, which is close to the observed source signature at the HUN site in the heating period (Sherwood et al., 2017) (Figure 5b).

Plots of the wind direction data and the corresponding measured CH_4 mole fraction or $\delta^{13}C_{CH4}$ value, also show differences between the vegetation growth periods and heating periods (Figure 6). During the heating period (Figures 6b and 6d), the prevailing wind direction is northern, where Austrian, Slovakian,

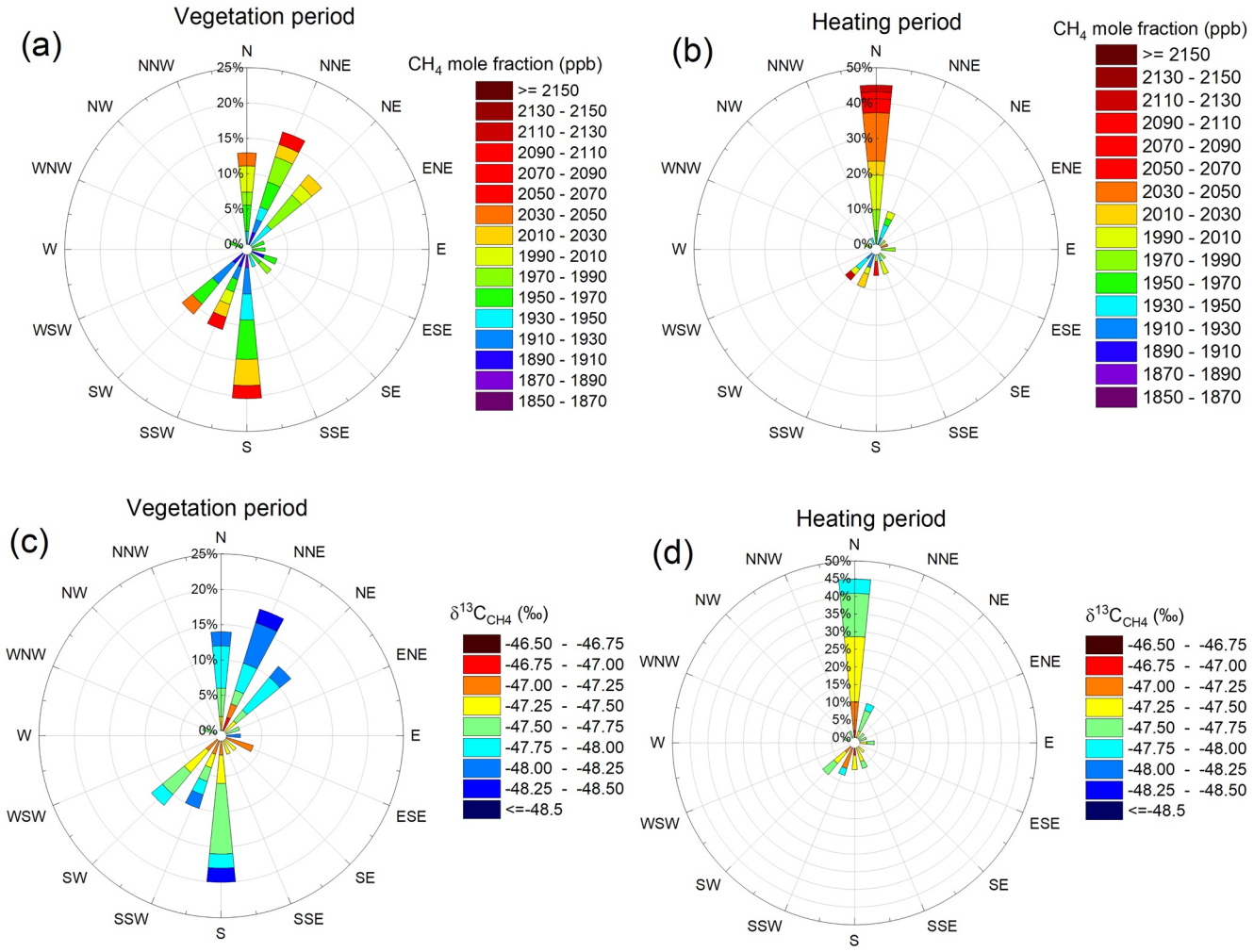

Figure 6. Plots by wind direction and measured CH_4 or $\delta^{13}C_{CH4}$. (a) For the vegetation period by wind direction and CH_4 mole fraction. (b) For the heating period by the wind direction and CH_4 mole fraction. (c) For the vegetation period by the wind direction and $\delta^{13}C_{CH4}$. (d) For the heating period by the wind direction and $\delta^{13}C_{CH4}$.

and Hungarian industrial areas are located, and 10% of the measurements are markedly enriched, with a ≥−47‰ $\delta^{13}C_{CH4}$ signal observed from this direction during the heating period. The wind pattern and source area during the vegetation period is more diverse, the plot shows dominant source areas at the NE and S (Figures 6a and 6c). Furthermore, the southern areas not as industrialized as the northern areas of Hungary. At the northeastern direction, at Mihályi and Répcelak, there is Hungary's one of the highest industrial CH_4 emitter facility, where the $\delta^{13}C_{CH4}$ of the emitted methane can be around −50.0‰ (Palcsu et al., 2014). However, during the vegetation period, biological emission with depleted $\delta^{13}C_{CH4}$ is not negligible what was observed from almost every direction in this period.

3.2. Sector Analysis Identification of CH_4 Emission Source Regions

Using each of the measured CH_4 mole fraction and $\delta^{13}C_{CH4}$ values coupled with the trajectories, CWT maps show the typical, mean value in the grid cells in different areas. Using the CWT algorithm, the potential source areas can be detected. The calculated mean values by the CWT algorithm (Formula #2 above) are shown in Figures S7 and S8. The trajectory distribution indicates dominant western source regions at the HUN and MHD sites. The stations have their own, distinct dominant source regions with negligible overlap (Figures 7 and S8).

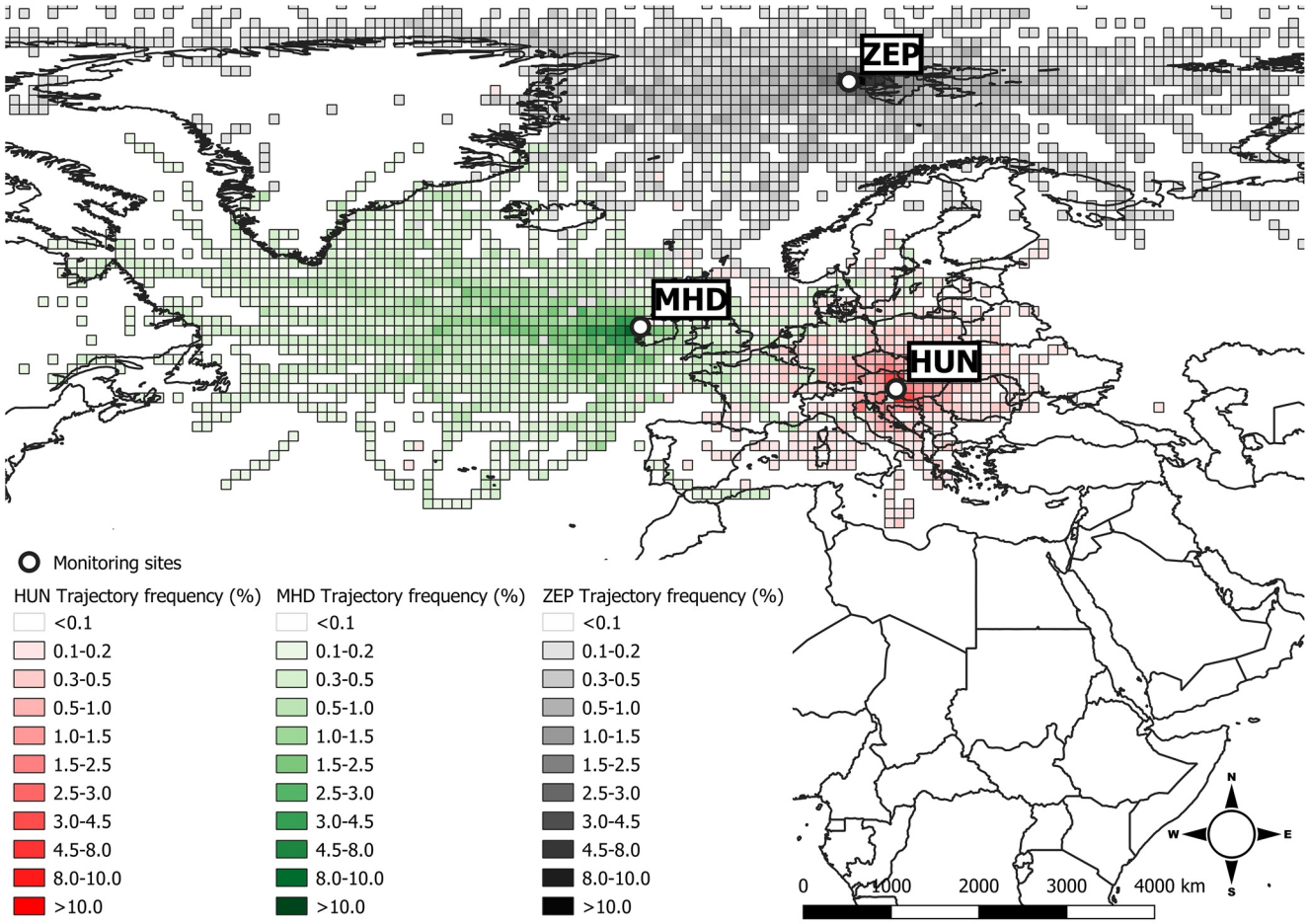

Figure 7. Trajectory frequency of Hegyhátsál, Hungary (HUN). Mace Head, Ireland (MHD) and Zeppelin, Svalbard (ZEP) sites. The colored grid cells show the frequency of the trajectories compared to all trajectories at the different sites. The red color scale shows the HUN. The green color scale shows the MHD. The gray color scale shows the ZEP site's color scale.

The following typical source regions were identified in the continental, marine, and polar areas, which are referred to in Figures 8 and S10:

1. The western region (Figures 8a, 8b, and S7), from which air masses had slightly elevated CH_4 mole fraction (<2,000 ppb), compared to the Mediterranean Sea, Adriatic Sea coastal region (<1,960 ppb). Western Europe is densely populated and with large-scale use of gas for heating and power, as well as large ruminant populations. In this area, at the western European region, relatively homogeneously high methane emission is present in the EDGAR v5.0 inventory, generally more than 9×10^{-11} kg $CH_4/m^2/s$ (EDGAR, 2019). At these areas, the agricultural and industrial (fossil) emission is also high. Our model data confirms this elevated methane emission in this region, but a dominant $\delta^{13}C_{CH4}$ signal can not be observed. The $\delta^{13}C_{CH4}$ isotopic composition of the air masses arriving from these areas is around −47.5‰, while the global bulk ambient air is between −47.8 and −47.2‰ with fractionation. The inventory shows that the transport-related CH_4 emission is the only anthropogenic emission in the Adriatic Sea, which is not as high as in the CH_4 emission at the onshore areas
2. The eastern region was the origin of air masses with higher CH_4 mixing ratios (>2,000 ppb) coupled with somewhat enriched, even higher than −47.3‰ $\delta^{13}C_{CH4}$ signals (Figures 8a, 8b, S7 and S8). This region includes major ruminant populations and the largest river wetland in Europe, the Danube Delta (Gómez-Baggethun et al., 2019). Methane emissions from wetlands and agricultural ruminants typically have a relatively negative $\delta^{13}C_{CH4}$ source signature (Dlugokencky et al., 2011; Ganesan et al., 2018). The middle and northeast Pannonian Basin region is industrialized, and with multiple emission sources in the region of Budapest (Bergamaschi et al., 2018). Note also that aerosol studies have shown that

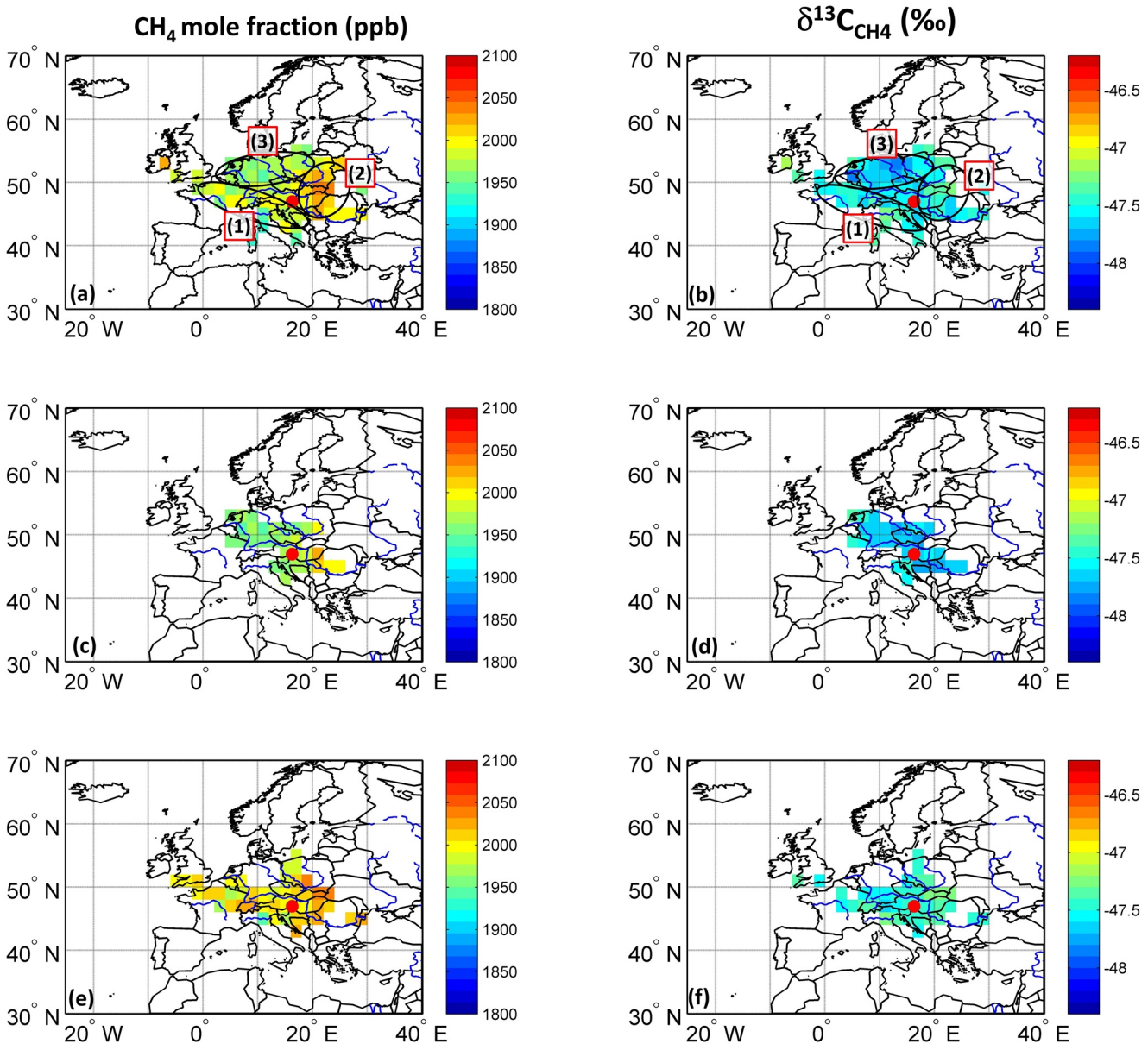

Figure 8. Methane mole fraction and $\delta^{13}C_{CH4}$ ratio concentration weighted trajectory (CWT) maps. The left column shows the mean CH_4 mole fraction for each 2° grid cell containing a minimum of four trajectories. The right column shows the mean $\delta^{13}C_{CH4}$ signal for each 2° grid cell containing minimum four trajectories (a) Mole fraction (ppb) CWT map at HUN site for the whole investigated period; (b) $\delta^{13}C_{CH4}$ CWT map at HUN site for the whole investigated period (c) Mole fraction (ppb) CWT map at HUN site for the vegetation period; (d) $\delta^{13}C_{CH4}$ CWT map at HUN site for the vegetation period (e) Mole fraction (ppb) CWT map at HUN site for the heating period; (f) $\delta^{13}C_{CH4}$ CWT map at HUN site for the heating period. The red dots show the locations of the monitoring site.

biomass burning is a significant contributor to atmospheric particulate matter around Budapest (Salma et al., 2017, 2020). Comparison with EDGAR v5.0 inventory also confirms this hypothesis, as Budapest and its agglomeration is a large contributor to the Hungarian methane budget (3×10^{-9} kg $CH_4/m^2/s$). However, the Carpathians have dominant natural methane sources as well, not identified by the EDGAR v5.0 inventory. Saunois et al. (2020) show large CH_4 emissions in the Eastern Carpathians (locally over 1×10^{-7} kg $CH_4/m^2/s$). Our results show somewhat elevated $\delta^{13}C_{CH4}$ from this source region. Kotarba and Nagao (2008) found that methane from the Polish and Ukrainian Carpathian region generally has an elevated $\delta^{13}C_{CH4}$ ratio, even more enriched than −40‰. Baciu et al. (2018) also show that the $\delta^{13}C_{CH4}$ ratio of Carpathian emissions is generally enriched compared to the bulk atmospheric $\delta^{13}C_{CH4}$ ratio

3. The northwestern and northern central European regions (Figures 8a, 8b, and S8). In the air from this region, the CH_4 mole fraction is not elevated significantly, but the air masses have a $\delta^{13}C_{CH4}$ isotopic signature that is, the most depleted compared to the surrounding sectors (<−47.75‰ $\delta^{13}C_{CH4}$). This area has both large-scale industrial, natural gas related CH_4 emission and also intensively cultivated areas with high ruminant populations, and widespread cattle and pig manure emission, as well as large landfills and waste systems. The EDGAR v5.0 inventory shows relatively high CH_4 emission (even more than 4×10^{-10} kg/m^2/s) in Belgium and Netherland, where the main contributions are the industrial (fossil) and agricultural emissions, but waste-related methane emission is also higher in this region. The biological and agricultural CH_4 sources have significantly depleted $\delta^{13}C_{CH4}$ isotopic signatures (Sherwood et al., 2017) and other studies show that this area has emission sources with dominantly negative $\delta^{13}C_{CH4}$ isotopic signature (Menoud et al., 2020; Röckmann et al., 2016). In the studies of Röckmann et al. (2016) and Menoud et al. (2020) values more negative than −49.5‰ $\delta^{13}C_{CH4}$ were generally measured in Cabauw and Lutjewad. The mix of the different CH_4 sources with depleted $\delta^{13}C_{CH4}$ at the Northern European area results in a negative $\delta^{13}C_{CH4}$ source signature for this area, as our model results also show

The differentiated CWT maps illustrate the higher CH_4 levels in the heating period (Figure 8e). During the vegetation period, the CWT analysis shows lower CH_4 mole fraction values over the northern and western European areas and the $\delta^{13}C_{CH4}$ source signature is slightly depleted, lower than −47.5‰ (Figures 8c and 8d), compared to the observed signature during the heating period, when the $\delta^{13}C_{CH4}$ source signature is higher than −47.5‰ (Figure 8f). This coupled with the Miller-Tans plot analysis shows dominant industrial gas and residential heating related CH_4 emission during the winter. The deeper PBL during the vegetation period favors the lower CH_4 mole fraction values, but the depleted $\delta^{13}C_{CH4}$ signature suggests mainly biological, microbial emission during this period.

There is no significant correlation between our modeled spatial data and EDGAR v5.0 inventory, which shows that the emission data included in the inventory only slightly affect the measured value at the HUN site. The main influencing factors may be the local changes of the PBL and the residential heating during the winter. This claim is supported by the local CO data (Petron et al., 2019) and the Miller-Tans plot results. The measured CH_4 mole fraction values are close to the values at the MHD and ZEP sites during the vegetation period, the difference is higher during the heating period, but the $\delta^{13}C_{CH4}$ values are not shifted significantly. This suggests also that meteorology can be the main factor in the changes of the local CH_4 values.

4. Conclusions

Methane mole fractions in air masses from continental source areas are generally higher compared with contemporaneous values measured by the coastal and polar clean air sites. At the Hegyhátsál site, Hungary, methane mole fraction was constantly above 2,000 ppb in the winter heating period between 2013 and 2015. The CH_4 level at the Hungarian site is comparable with other European continental sites, such as Heidelberg and Gif-sur-Yvette, but greater than at the continental background Jungfraujoch and also greater than an American continental background station, Niwot Ridge. The results show that the HUN station is suitable for regional methane studies as it samples both clean and polluted air masses, enabling the identification of emission source areas.

The mean $\delta^{13}C_{CH4}$ ratio over 2013–2015 observed in Hegyhátsál is −47.5 ± 0.6‰, similar to the means at the Zeppelin and Mace Head observatory sites over this period, −47.5 ± 0.4‰ and −47.5 ± 0.5‰, respectively (the error is the 2σ stdev of the measurements over the investigated period). The Miller-Tans plots show a more enriched signature during the heating period in Europe over winter (−46.3 ± 1.6‰) when fossil fuel and pyrogenic emissions dominate, compred with the vegetation period (−52.5 ± 1.9‰) when there is a larger influence from biogenic sources.

Using sector analysis of concentration-weighted back trajectories, potential emission source regions were studied. This backward trajectory modeling and potential source area analysis identified inputs to methane mixing ratio and $^{13}C/^{12}C$ ratio at the Hegyhátsál monitoring site from distinct areas, such as western, northern, and northwestern coastal European regions. The EDGAR v5.0 inventory also shows a contribution from these areas. We found a CH_4 contribution from the Eastern Hungarian area as well, which can be a mix of industrial and geological CH_4 emissions.

Boundary layer effects in the local, isolated environmental condition of the Pannonian Basin also play a major role in controlling methane mole fraction in the ambient air in the heating period.

Data Availability Statement

We thank Edward J. Dlugokencky and NOAA-ESRL for their published CH_4 mole fraction data set https://www.esrl.noaa.gov/gmd/dv/data. We thank Bruce Vaughn, Sylvia Michel, and the University of Colorado - INSTAAR for their published $\delta^{13}C_{CH4}$ data set https://instaar.colorado.edu/about-us/visiting-instaar/.

Acknowledgments
The research was supported by the European Union and the State of Hungary, co-financed by the European Regional Development Fund in the project of GINOP-2.3.2-15-2016-00009 "ICER." The research leading to these results has received funding from the European Community's Seventh Framework Programme (FP7/2007–2013) in the InGOS project under grant agreement no. 284274. The work of László Haszpra was supported by the National Scientific Research Fund OTKA K129118. RHUL measurement was supported by the EU *Geomon* and *InGOS* projects and NERC projects NE/N016238/1 *MOYA: The Global Methane Budget* and NE/P019641/1, *New methodologies for removal of methane from the atmosphere*, awarded to E. G. Nisbet, D. Lowry and R. E. Fisher. Supported by the ÚNKP-20-3 New National Excellence Program of the Ministry for Innovation and Technology from the source of the National Research, Development and Innovation Fund. The authors gratefully acknowledge the NOAA Air Resources Laboratory for the provision of the HYSPLIT transport and dispersion model and/or READY website (http://www.ready.noaa.gov) used in this publication.

References

Baciu, C., Ionescu, A., & Etiope, G. (2018). Hydrocarbon seeps in Romania: Gas origin and release to the atmosphere. *Marine and Petroleum Geology*, *89*, 130–143. https://doi.org/10.1016/j.marpetgeo.2017.06.015

Bartholy, J., & Radics, K. (2005). Wind profile analyses and atmospheric stability over a complex terrain in southwestern part of Hungary. *Physics and Chemistry of the Earth*, *30*(1–3), 195–200. https://doi.org/10.1016/j.pce.2004.08.013

Bergamaschi, P., Karstens, U., Manning, A. J., Saunois, M., Tsuruta, A., Berchet, A., et al. (2018). Inverse modelling of European CH_4 emissions during 2006–2012 using different inverse models and reassessed atmospheric observations. *Atmospheric Chemistry and Physics*, *18*(2), 901–920. https://doi.org/10.5194/acp-18-901-2018

Bertelsen, N., & Mathiesen, B. V. (2020). EU-28 residential heat supply and consumption: Historical development and status. *Energies*, *13*(8), 1894. https://doi.org/10.3390/en13081894

Brownlow, R., Lowry, D., Fisher, R. E., France, J. L., Lanoisellé, M., White, B., et al. (2017). Isotopic ratios of tropical methane emissions by atmospheric measurement. *Global Biogeochemical Cycles*, *31*(9), 1408–1419. https://doi.org/10.1002/2017GB005689

Chang, J., Peng, S., Ciais, P., Saunois, M., Dangal, S. R. S., Herrero, M., et al. (2019). Revisiting enteric methane emissions from domestic ruminants and their $\delta^{13}CCH_4$ source signature. *Nature Communications*, *10*(1), 1–14. https://doi.org/10.1038/s41467-019-11066-3

Davis, J. S. (1986). *Statistics and data analysis in geology*. John Wiley & Sons, Ltd.

Dlugokencky, E. (Ed.). (2021). *Global CH_4 monthly means*. Retrieved from https://gml.noaa.gov/ccgg/trends_ch4/

Dlugokencky, E., Crottwell, A., Mund, J., Crotwell, M., & Thoning, K. (2019). *Atmospheric methane dry air mole fractions from the NOAA ESRL carbon cycle cooperative global air sampling network, 1983–2018,Version: 2019-07*. Retrieved from https://doi.org/10.15138/VNCZ-M766

Dlugokencky, E., Mund, J. W., Crotwell, A. M., Crotwell, M. J., & Thoning, K. W. (2021). Atmospheric carbon dioxide dry air mole fractions from the NOAA GML carbon cycle cooperative global air sampling network, 1968–2019, Version: 2021-02. https://doi.org/10.15138/wkgj-f21

Dlugokencky, E., Nisbet, E., Fisher, R., & Lowry, D. (2011). Global atmospheric methane: Budget, changes and dangers. *Philosophical Transactions of the Royal Society A: Mathematical, Physical & Engineering Sciences*, *369*, 2058–2072. https://doi.org/10.1098/rsta.2010.0341

Draxler, R. R. (1998). An overview of the HYSPLIT_4 modelling system for trajectories. *Australian Meteorological Magazine*, *47*, 295–308.

Ebisuzaki, W. (1997). A method to estimate the statistical significance of a correlation when the data are serially correlated. *Journal of Climate*, *10*(9), 2147–2153. https://doi.org/10.1175/1520-0442(1997)010<2147:AMTETS>2.0.CO;2

EDGAR. (2019). Retrieved from https://edgar.jrc.ec.europa.eu/report_2019

Etminan, M., Myhre, G., Highwood, E. J., & Shine, K. P. (2016). Radiative forcing of carbon dioxide, methane, and nitrous oxide: A significant revision of the methane radiative forcing. *Geophysical Research Letters*, *43*(24), 614–712. https://doi.org/10.1002/2016GL071930

Fisher, R., Lowry, D., Wilkin, O., Sriskantharajah, S., & Nisbet, E. G. (2006). High-precision, automated stable isotope analysis of atmospheric methane and carbon dioxide using continuous-flow isotope-ratio mass spectrometry. *Rapid Communications in Mass Spectrometry*, *20*(2), 200–208. https://doi.org/10.1002/rcm.2300

Fisher, R. E., France, J. L., Lowry, D., Lanoisellé, M., Brownlow, R., Pyle, J. A., et al. (2017). Measurement of the 13C isotopic signature of methane emissions from northern European wetlands. *Global Biogeochemical Cycles*, *31*(3), 605–623. https://doi.org/10.1002/2016GB005504

France, J. L., Cain, M., Fisher, R. E., Lowry, D., Allen, G., O'Shea, S. J., et al. (2016). Measurements of $\delta^{13}C$ in CH_4 and using particle dispersion modeling to characterize sources of Arctic methane within an air mass. *Journal of Geophysical Research: Atmospheres*, *121*(23), 257–314. https://doi.org/10.1002/2016JD026006

Fung, I., John, J., Lerner, J., Matthews, E., Prather, M., Steele, L. P., & Fraser, P. J. (1991). Three-dimensional model synthesis of the global methane cycle. *Journal of Geophysical Research*, *96*(D7), 13033–13065. https://doi.org/10.1029/91JD01247

Ganesan, A. L., Stell, A. C., Gedney, N., Comyn-Platt, E., Hayman, G., Rigby, M., et al. (2018). Spatially resolved isotopic source signatures of wetland methane emissions. *Geophysical Research Letters*, *45*(8), 3737–3745. https://doi.org/10.1002/2018GL077536

García, M. Á., Sánchez, M. L., Pérez, I. A., Ozores, M. I., & Pardo, N. (2016). Influence of atmospheric stability and transport on CH_4 concentrations in northern Spain. *The Science of the Total Environment*, *550*, 157–166. https://doi.org/10.1016/j.scitotenv.2016.01.099

Gómez-Baggethun, E., Tudor, M., Doroftei, M., Covaliov, S., Năstase, A., Onără, D.-F., et al. (2019). Changes in ecosystem services from wetland loss and restoration: An ecosystem assessment of the Danube Delta (1960–2010). *Ecosystem Services*, *39*(1432), 100965. https://doi.org/10.1016/j.ecoser.2019.100965

Górka, M., Lewicka-Szczebak, D., Fuß, R., Jakubiak, M., & Jędrysek, M.O. (2014). Dynamics and origin of atmospheric CH_4 in a Polish metropolitan area characterized by wetlands. *Applied Geochemistry*, *45*, 72–81. http://doi.org/10.1016/j.apgeochem.2014.03.007

Haszpra, L., Barcza, Z., Davis, K. J., & Tarczay, K. (2005). Long-term tall tower carbon dioxide flux monitoring over an area of mixed vegetation. *Agricultural and Forest Meteorology*, *132*(1–2), 58–77. https://doi.org/10.1016/j.agrformet.2005.07.002

Haszpra, L., Barcza, Z., Szilágyi, I., Dlugokencky, E., & Tans, P. (2008). Trends and temporal variations of major greenhouse gases at a rural site in central Europe. In *Atmospheric greenhouse gases: The Hungarian perspective* (Vol. 42, pp. 29–47). Dordrecht. Springer Netherlands. https://doi.org/10.1007/978-90-481-9950-1_3

Haszpra, L., Ferenczi, Z., & Barcza, Z. (2019). Estimation of greenhouse gas emission factors based on observed covariance of CO_2, CH_4, N_2O and CO mole fractions. *Environmental Sciences Europe*, *31*(1), 95. https://doi.org/10.1186/s12302-019-0277-y

Hsu, Y.-K., Holsen, T. M., & Hopke, P. K. (2003). Comparison of hybrid receptor models to locate PCB sources in Chicago. *Atmospheric Environment*, *37*(4), 545–562. https://doi.org/10.1016/S1352-2310(02)00886-5

InGOS. (2015a). *InGOS CH_4 release* (p. 2000). Heidelberg. Retrieved from https://hdl.handle.net/11676/SuJXuSUDpxA9__QN-XnjLoOb
InGOS. (2015b). *InGOS CH_4 Release, Gif sur Yvette (7.0 m), 2013-07-01–2015-06-30*. Retrieved from https://hdl.handle.net/11676/SuJXuSUDpxA9__QN-XnjLoOb
InGOS. (2015c). *InGOS CH_4 release, Jungfraujoch (5.0 m), 2005-01-01–2015-06-01*. Retrieved from https://hdl.handle.net/11676/F5LbbXnWZ9sW5ODzzMCOALJA
IPCC. (2018). *Summary for Policymakers*. In: *Global Warming of 1.5°C. An IPCC Special Report on the impacts of global warming of 1.5°C above pre-industrial levels and related global greenhouse gas emission pathways, in the context of strengthening the global response to. Draft report, 48th IPCC, Incheon, Korea, 6 Oct. 2018*. Retrieved from https://report.ipcc.ch/sr15/pdf/sr15_spm_final.pdf%0Ahttp://www.ipcc.ch/report/sr15/
Kirschke, S., Bousquet, P., Ciais, P., Saunois, M., Canadell, J. G., Dlugokencky, E. J., et al. (2013). Three decades of global methane sources and sinks. *Nature Geoscience*, *6*(10), 813–823. https://doi.org/10.1038/ngeo1955
Kotarba, M. J., & Nagao, K. (2008). Composition and origin of natural gases accumulated in the Polish and Ukrainian parts of the Carpathian region: Gaseous hydrocarbons, noble gases, carbon dioxide and nitrogen. *Chemical Geology*, *255*(3–4), 426–438. https://doi.org/10.1016/j.chemgeo.2008.07.011
László, E., Palcsu, L., & Leelőssy, Á. (2020). Estimation of the solar-induced natural variability of the tritium concentration of precipitation in the Northern and Southern Hemisphere. *Atmospheric Environment*, *233*, 117605. https://doi.org/10.1016/j.atmosenv.2020.117605
Lowry, D., Fisher, R. E., France, J. L., Coleman, M., Lanoisellé, M., Zazzeri, G., et al. (2020). Environmental baseline monitoring for shale gas development in the UK: Identification and geochemical characterisation of local source emissions of methane to atmosphere. The *Science of the Total Environment*, *708*, 134600. https://doi.org/10.1016/j.scitotenv.2019.134600
Maheras, P., Tolika, K., Anagnostopoulou, C., Makra, L., Szpirosz, K., & Károssy, C. (2018). Relationship between mean and extreme precipitation and circulation types over Hungary. *International Journal of Climatology*, *38*(12), 4518–4532. https://doi.org/10.1002/joc.5684
Major, I., Haszpra, L., Rinyu, L., Futó, I., Bihari, Á., Hammer, S., et al. (2018). Temporal variation of atmospheric fossil and modern CO_2 excess at a central European rural tower station between 2008 and 2014. *Radiocarbon*, *60*(5), 1285–1299. https://doi.org/10.1017/RDC.2018.79
Mattey, D. P., Fisher, R., Atkinson, T. C., Latin, J.-P., Durrell, R., Ainsworth, M., et al. (2013). Methane in underground air in Gibraltar karst. *Earth and Planetary Science Letters*, *374*, 71–80. https://doi.org/10.1016/j.epsl.2013.05.011
Menoud, M., Veen, C. V. D, Scheeren, B., Chen, H., Szénási, B., Morales, R. P., et al. (2020). Characterisation of methane sources in Lutjewad, The Netherlands, using quasi-continuous isotopic composition measurements. *Tellus Series B Chemical and Physical Meteorology*, *72*(1), 1–20. https://doi.org/10.1080/16000889.2020.1823733
Miller, J. B., & Tans, P. P. (2003). Calculating isotopic fractionation from atmospheric measurements at various scales. *Tellus Series B Chemical and Physical Meteorology*, *55*(2), 207–214. https://doi.org/10.1034/j.1600-0889.2003.00020.x
Nisbet, E. G., Dlugokencky, E. J., Manning, M. R., Lowry, D., Fisher, R. E., France, J. L., et al. (2016). Rising atmospheric methane: 2007–2014 growth and isotopic shift. *Global Biogeochemical Cycles*, *30*(9), 1356–1370. https://doi.org/10.1002/2016GB005406
Nisbet, E. G., Manning, M. R., Dlugokencky, E. J., Fisher, R. E., Lowry, D., Michel, S. E., et al. (2019). Very strong atmospheric methane growth in the 4 years 2014–2017: Implications for the Paris agreement. *Global Biogeochemical Cycles*, *33*(3), 318–342. https://doi.org/10.1029/2018GB006009
Palcsu, L., Morgenstern, U., Sültenfuss, J., Koltai, G., László, E., Temovski, M., et al. (2018). Modulation of cosmogenic tritium in meteoric precipitation by the 11-year cycle of solar magnetic field activity. *Scientific Reports*, *8*(1), 12813. https://doi.org/10.1038/s41598-018-31208-9
Palcsu, L., Veto, I., Futó, I., Vodila, G., Papp, L., & Major, Z. (2014). In-reservoir mixing of mantle-derived CO_2 and metasedimentary CH_4-N_2 fluids - Noble gas and stable isotope study of two multistacked fields (Pannonian Basin System, W-Hungary). *Marine and Petroleum Geology*, *54*, 216–227. https://doi.org/10.1016/j.marpetgeo.2014.03.013
Petron, G., Crotwell, A., Dlugokencky, E., & Mund, J. (2019). Atmospheric carbon monoxide dry air mole fractions from the NOAA ESRL carbon cycle cooperative global air sampling network, 1988–2018, *Version: 2*. Retrieved from https://doi.org/10.15138/33bv-s284
Quay, P. D., King, S. L., Stutsman, J., Wilbur, D. O., Steele, L. P., Fung, I., et al. (1991). Carbon isotopic composition of atmospheric CH_4 : Fossil and biomass burning source strengths. *Global Biogeochemical Cycles*, *5*(1), 25–47. https://doi.org/10.1029/91GB00003
Radics, K., & Bartholy, J. (2008). Estimating and modelling the wind resource of Hungary. *Renewable and Sustainable Energy Reviews*, *12*(3), 874–882. https://doi.org/10.1016/j.rser.2006.10.009
Rigby, M., Montzka, S. A., Prinn, R. G., White, J. W. C., Young, D., O'Doherty, S., et al. (2017). Role of atmospheric oxidation in recent methane growth. *Proceedings of the National Academy of Sciences of the United States of America*, *114*(21), 5373–5377. https://doi.org/10.1073/pnas.1616426114
Röckmann, T., Eyer, S., Veen, C. V. D, Popa, M. E., Tuzson, B., Monteil, G., et al. (2016). In situ observations of the isotopic composition of methane at the Cabauw tall tower site. *Atmospheric Chemistry and Physics*, *16*(16), 10469–10487. https://doi.org/10.5194/acp-16-10469-2016
Salma, I., Németh, Z., Weidinger, T., Maenhaut, W., Claeys, M., Molnár, M., et al. (2017). Source apportionment of carbonaceous chemical species to fossil fuel combustion, biomass burning and biogenic emissions by a coupled radiocarbon–levoglucosan marker method. *Atmospheric Chemistry and Physics*, *17*(22), 13767–13781. https://doi.org/10.5194/acp-17-13767-2017
Salma, I., Vasanits-zsigrai, A., Machon, A., Varga, T., Major, I., & Gergely, V., Molnár, M. (2020). Fossil fuel combustion, biomass burning and biogenic sources of fine carbonaceous aerosol in the Carpathian Basin. *Atmospheric Chemistry and Physics*, *20*, 4295–4312. https://doi.org/10.5194/acp-20-4295-2020
Saunois, M., Bousquet, P., Poulter, B., Peregon, A., Ciais, P., Canadell, J. G., et al. (2016). The global methane budget 2000–2012. *Earth System Science Data*, *8*(2), 697–751. https://doi.org/10.5194/essd-8-697-2016
Saunois, M., Stavert, R. A., Poulter, B., Bousquet, P., Canadell, G., Jackson, R. B., et al. (2020). The global methane budget 2000–2017. *Earth System Science Data*, *12*(3), 1561–1623. https://doi.org/10.5194/essd-12-1561-2020
Schaefer, H., Fletcher, S. E. M., Veidt, C., Lassey, K. R., Brailsford, G. W., Bromley, T. M., et al. (2016). A 21st-century shift from fossil-fuel to biogenic methane emissions indicated by 13CH4. *Science*, *352*(6281), 80–84. https://doi.org/10.1126/science.aad2705
Schwietzke, S., Sherwood, O. A., Bruhwiler, L. M. P., Miller, J. B., Etiope, G., Dlugokencky, E. J., et al. (2016). Upward revision of global fossil fuel methane emissions based on isotope database. *Nature*, *538*(7623), 88–91. https://doi.org/10.1038/nature19797
Sherwood, O. A., Schwietzke, S., Arling, V. A., & Etiope, G. (2017). Global inventory of gas geochemistry data from fossil fuel, microbial and burning sources, version 2017. *Earth System Science Data*, *9*(2), 639–656. https://doi.org/10.5194/essd-9-639-2017
Stull, R. (1988). An introduction to boundary layer meteorology. https://doi.org/10.1007/978-94-009-3027-8

Su, L., Yuan, Z., Fung, J. C. H., & Lau, A. K. H. (2015). A comparison of HYSPLIT backward trajectories generated from two GDAS datasets. *The Science of the Total Environment*, *506*(507), 527–537. https://doi.org/10.1016/j.scitotenv.2014.11.072

Turner, A. J., Frankenberg, C., Wennberg, P. O., & Jacob, D. J. (2017). Ambiguity in the causes for decadal trends in atmospheric methane and hydroxyl. *Proceedings of the National Academy of Sciences of the United States of America*, *114*(21), 5367–5372. https://doi.org/10.1073/pnas.1616020114

Tyler, S. C., Rice, A. L., & Ajie, H. O. (2007). Stable isotope ratios in atmospheric CH_4: Implications for seasonal sources and sinks. *Journal of Geophysical Research*, *112*(D3), D03303. https://doi.org/10.1029/2006JD007231

von Engeln, A., & Teixeira, J. (2013). A planetary boundary layer height climatology derived from ECMWF reanalysis data. *Journal of Climate*, *26*, 6575–6590. https://doi.org/10.1175/JCLI-D-12-00385.1

Wang, Y. Q., Zhang, X. Y., & Draxler, R. R. (2009). TrajStat: GIS-based software that uses various trajectory statistical analysis methods to identify potential sources from long-term air pollution measurement data. *Environmental Modelling & Software*, *24*(8), 938–939. https://doi.org/10.1016/j.envsoft.2009.01.004

Webster, K. D., Drobniak, A., Etiope, G., Mastalerz, M., Sauer, P. E., & Schimmelmann, A. (2018). Subterranean karst environments as a global sink for atmospheric methane. *Earth and Planetary Science Letters*, *485*, 9–18. https://doi.org/10.1016/j.epsl.2017.12.025

White, J., Vaughn, B., & Michel, S. (2018). University of Colorado, Institute of Arctic and Alpine Research (INSTAAR), Stable Isotopic Composition of Atmospheric Methane (13C) from the NOAA ESRL Carbon Cycle Cooperative Global Air Sampling Network 1998–2017, Version 2018-09-24.

Worden, J. R., Bloom, A. A., Pandey, S., Jiang, Z., Worden, H. M., Walker, T. W., et al. (2017). Reduced biomass burning emissions reconcile conflicting estimates of the post-2006 atmospheric methane budget. *Nature Communications*, *8*(1), 1–11. https://doi.org/10.1038/s41467-017-02246-0

Zazzeri, G., Lowry, D., Fisher, R. E., France, J. L., Lanoisellé, M., Grimmond, C. S. B., & Nisbet, E. G. (2017). Evaluating methane inventories by isotopic analysis in the London region. *Scientific Reports*, *7*(1), 4854. https://doi.org/10.1038/s41598-017-04802-6

Zazzeri, G., Lowry, D., Fisher, R. E., France, J. L., Lanoisellé, M., Kelly, B. F. J., et al. (2016). Carbon isotopic signature of coal-derived methane emissions to the atmosphere: From coalification to alteration. *Atmospheric Chemistry and Physics*, *16*(21), 13669–13680. https://doi.org/10.5194/acp-16-13669-2016